Synthesis of highly porous activated carbon nanofibers derived from bamboo waste materials for application in supercapacitor

Rakhmawati Farma[1,*] , Aldila Putri[1], Erman Taer[1], Awitdrus Awitdrus[1], and Apriwandi Apriwandi[1]

[1] *Department of Physics, University of Riau, Simpang Baru, Riau 28293, Indonesia*

ABSTRACT

Sample activated carbon electrodes sourced from bamboo materials are synthesized using a combination of chemical and physical activation and applied in the production of supercapacitor cells. This study, therefore, focuses on the carbonization temperatures of 600 °C (BA-600), 700 °C (BA-700), 800 °C (BA-800), and 900 °C (BA-900). Subsequently, the physical properties of activated carbon were characterized, using thermogravimetry analysis (TGA), X-ray diffraction (XRD), scanning electron microscope (SEM), energy-dispersive X-ray (EDX), and Brunauer–Emmet–Teller (BET). All samples demonstrate highly porous carbon on the surface of the electrode. In addition, carbon fiber also presented in BA-700 and BA-800 samples had an average diameter of 0.17 μm and 0.06 μm. The electrochemical characteristics were evaluated using cyclic voltammetry (CV) method, and 800 °C was identified as the optimum temperature condition for carbonization. Conversely, the highest specific capacitance was demonstrated by the BA-800 electrode, which demonstrated a value of about 174 F g^{-1}, with high specific surface area of 1137.86 m^2 g^{-1}.

1 Introduction

The development of increasingly modern technology creates high energy utility, leading to the consequent reduction in the available main energy source. Therefore, it is pertinent to explore other alternatives necessary to meet up with the demand. Several of the alternative energy sources developed by the researchers are wind, solar, geothermal, ocean waves, coal, peat, biomass, and others [1]. Therefore, energy-storage devices are needed, as a form of utility to support the performance and utilization of alternative energy sources, including batteries, capacitors, supercapacitors, and fuel cells [2, 3].

Particularly, supercapacitor are electrochemical devices consisting of electrodes, current collectors, electrolytes and separators, which possess special properties in the nature of energy and high power density, good durability, long life time, inexpensive, relatively charge/discharge times fast and safe to use

Address correspondence to E-mail: rfarma06@yahoo.co.id

Ⓐ Springer

[2, 4]. Furthermore, the energy and power density is determined by the type of electrode used, especially porous carbon material, which is possibly produced from biomass materials, including cotton [5], coconut husk [6], woods [7], and bamboo [8, 9]. These are very good considerations to be developed, due to the ease of acquisition, low production costs, and the ability to form pore structures.

In addition, bamboo is one of the usable materials, of which Indonesia has about 60 species, which is generally found growing from the lowlands to mountains at altitude of 300 m above sea level. Furthermore, raw bamboo has three main components that dominate 90% of its total mass, including cellulose, hemicellulose, and lignin are 73.83%, 12.49%, and 10.15%, respectively. Other minor components a fraction of aqueous extract and pectin [10, 11]. These components have the importance of providing high porous carbon with a good pore combination for the electrode material [8, 12]. In addition, the high cellulose component allows biomass to produce porous carbon with a nanomaterial structure, especially nanofibers [13]. Furthermore, the fiber component has a larger cell wall and lumen, which tends to be comparably narrower than other plant fibers, including those sourced from wood [14, 15]. Furthermore, the nanomaterials structure, particularly the nanofibers, contributes to improving the performance of the supercapacitor. This is due to the nanofibers could provide high conductivity to ensure high power density as well as an adequate pore size distribution consisting mostly of pores with an average pore size smaller than 1–2 nm increasing capacitance in aqueous or organic electrolytes [16]. However, the nanofiber structure preparation method for supercapacitor electrodes is still relatively more complex and requires synthetic materials such as PANI [17, 18]. Conversely, the porous structure is suitable for the adsorption and desorption of electrolyte ions without chemical reactions, while the high conductive properties ensures the possibility of performing quick charging [19]. This is conducted to facilitate the electrochemical process and further improve the performance of supercapacitors [20, 21].

Carbonization is a common method adopted in the synthesis of activated carbon, based on biomass materials, and the optimal temperature of carbonization is one of the influencing factors [19]. Furthermore, high values are implicated in elevated collision energies between the inert gas molecules and the atoms of biomass materials, resulting in the breaking of bonds between carbon and non-carbon atoms. This leads to the conversion of organic carbon content to porous carbon materials, and the best results occur at the optimum temperature of carbonization, which is unique to each type of biomass. Moreover, some previous studies have mentioned the conduction of similar experiment at specific temperatures ranging from 400 to 900 °C [22, 23].

In this study, we prepared activated carbon with nanofibers structure by using simple and facile method through chemical activation and pyrolysis process without the addition of synthetic materials such as conducting polymer and metal oxide. Moreover, the supercapacitor electrodes used in this research were synthesized from bamboo materials at carbonization temperature variations of 600 °C (BA-600), 700 °C (BA-700), 800 °C (BA-800), and 900 °C (BA-900). As results, the surface morphology of activated carbon reviewed high nanofiber structure with high specific surface area of 1137.86 m^2 g^{-1}. Furthermore, the electrochemical behavior has performed using cylic voltammetry in two-electrode system and it found excellent specific capacitance as high as 174 F g^{-1} in 1 M H_2SO_4 aqueous electrolyte at low scanning rate of 1 mV s^{-1}. All of these results confirmed that the great potential of bamboo was as excellent material for porous activated carbon as electrode material for supercapacitor.

2 Materials and methods

2.1 Preparation of activated carbon

The preparation of activated carbon was initiated with the process of cleaned and cut the bamboo waste, in order to facilitate the drying process. This involves sun-dried to attain a constant mass reduction within a period of 5–7 days. Subsequently, the sample is treated with pre-carbonization, using oven regulated at 200 °C for 1 h, followed by mashing to a powder of size < 53 μm through by milling and sifting. The carbon powder was chemically activated with 1 M potassium hydroxide (KOH), and converted into monoliths, using a Hydraulic press. In addition, the pyrolysis process is conducted using single step pyrolysis which begin with carbonization, involving the use of N_2 gas for 1 h with temperature variations of 600 °C, 700 °C, 800 °C, and 900 °C,

coded as sample BA-600, BA-700, BA- 800, and BA-900, and followed by physical activation process, which required employing CO_2 gas at 900 °C for 2.5 h. Finally, the carbon electrodes are arranged to form supercapacitor cells consisting of activated carbon electrodes, separators, and electrolytes [24].

2.2 Characterization of physical properties

The physical properties of the electrodes were characterized using several methods, including thermogravimetry analysis, X-ray diffraction, scanning electron microscopy, energy-dispersive X-ray, and N_2 gas absorption. Thermogravimetry analysis (TGA, Shimadzu TGA-50) was evaluated at a heating rate of 10 °C min^1 in the N_2 gas atmosphere. X-ray diffraction was reviewed microstructure by using Phillip X-Pert Pro PW3060/10 instrument in the 2θ angle range of 10°–60°. Scanning electron microscopy and energy-dispersive X-ray for surface morphology and chemical composition were performed by using JEOL JSM-6510 LA instrument, and N_2 gas absorption to ascertain the porosity properties by using Quantachrome TouchWiz v1.2 instrument at a liquid temperature of 77 K.

2.3 Characterization of electrochemical properties

Cyclic voltammetry method is popularly used to evaluate an electrodes capacitive property. This characterization was performed using a physic tool CV UR Rad-Er 5841 at a scan rate of 1 mV s^{-1} with the potential of 500 mV on a two-electrode system in 1 M H_2SO_4 solution. The supercapacitor cell was assembled by the coin-type which consists of the two-electrodes with monolith form without the addition of adhesive material, an egg duck shell membrane as separator, and aqueous electrolyte in 1 M H_2SO_4. The electrodes were prepared by polished the carbon monolith CPs which had been pyrolyzed to a certain thickness of 0.2 mm and placed in two pieces without binder materials. Subsequently, the measurement results are processed using CorrWare 2 software, in order to obtain data from the curve depicting the relationship between current and voltage.

3 Results and discussion

3.1 Density analysis

The carbonization process of N_2 gas affects the density of activated carbon electrodes, due to the inherent ability to modify the pore structure and surface area. Moreover, the diameter, thickness, and mass tend to change as a result of exposure to high temperatures, subsequently expanding pore diameter and forming new ones. These treatments ultimately change the sample density from 0.8654 g cm^{-3}, 0.9016 g cm^{-3}, 1.1495 g cm^{-3}, and 1.23333 g cm^{-3} to 0.85341 g cm^{-3}, 0.8639 g cm^{-3}, 1.00841 g cm^{-3}, and 1.05531 g cm^{-3} for BA-600, BA-700, BA-800, and BA-900, respectively. All samples show a decreased density after the pyrolysis process, Furthermore, the significance of the first stage in the carbonization process is to convert the raw material into char and developing initial pores and surface area. The physicochemical properties of raw char and the resulting pores are too small for practical applications. Therefore, improving the quality of specific surface areas and pore properties is achieved by physical activation at a high temperature of 900 °C with a CO_2 gas environment for 2.5 h. In addition, the values are theoretically expected to be the same, being that the samples were prepared using a standard method, hence the observed difference was attributed to the use of analog measurement instruments, which is very prone to errors in data reading. The comparison of density before and after the carbonization and physical activation process is shown in Fig. 1.
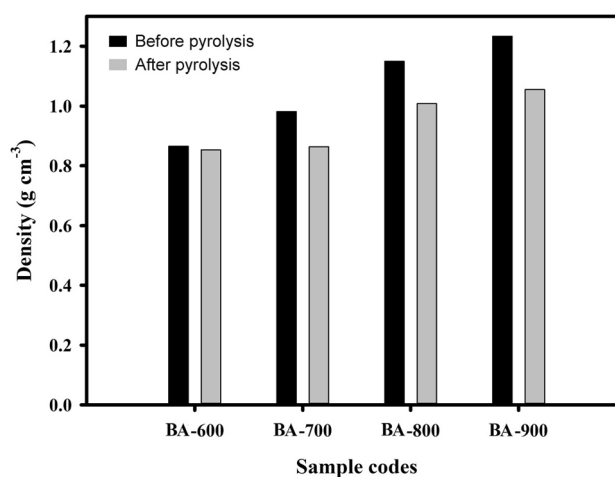

Fig. 1 Density of the activated carbon electrodes

Density is observed to have significantly declined at the end of the process, due to the evaporation of other elements asides carbon, including hydrogen, oxygen, and other impurities [24, 25]. Furthermore, physical activation improves the pore structure and surface of the sample, and also new ones are formed. The percentage of mass shrinkage is seen in Fig. 2, which shows a 1.199%, 11.77%, 14.109%, and 17.802% decline in density for sample BA-600, BA-700, BA-800, and BA-900, respectively. Moreover, an increase in carbonization temperature elevates this value, and the ultimate decline in density results from the reaction between carbon and N_2–CO_2 gas on the carbon surface, characterized by the evaporation of elements, subsequently causing pore expansion and the formation of new ones [26, 27].

3.2 Thermo-gravimetric analysis

The TGA profile of bamboo apus biomass shown in Fig. 3 consists of Differential Thermal Gravimetry (DTG) and Thermogravimetry (TG), which evaluate the effect of temperature rise. Furthermore, the pyrolysis of lignocellulose materials plays an important role as the first chemical step in the carbonization process, and a temperature range of 300–500 °C ensures the evaporation of hemicellulose, cellulose, and lignin [28]. Previous studies have confirmed volatility in most biomass components [29], which is necessary to identify the maximum mass shrinkage temperature for samples to be used for heat resistance in the carbonization process. At 104.8 °C, the TG curve of bamboo apus shows a value of 3.99%,
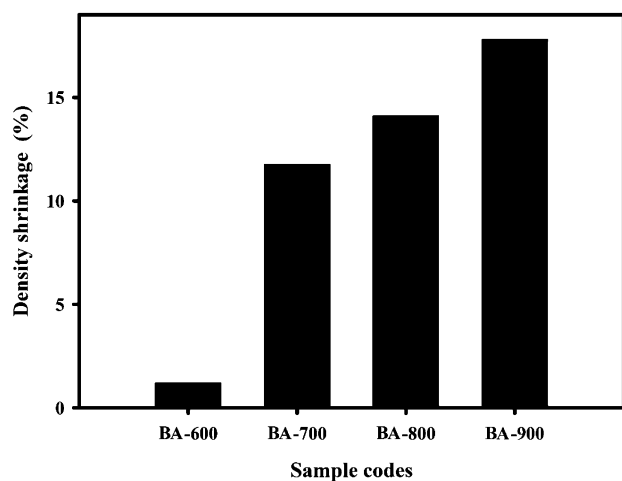
indicating the occurrence of water evaporation in the biomass, while 10.78% was recorded at 280.2 °C, designating the evaporation of hemicellulose and lignin [30]. In addition, cellulose, hemicellulose, and lignin components simultaneously vaporize at 366.2 °C, with a mass shrinkage of 44.57%, while 61.15% was recorded at 550.7 °C, indicating continuity in the evaporation of the lignin composition [30]. Conversely, the DTG curve demonstrates a significantly faster mass shrinkage at 338.7 °C, with a decomposition speed of 0.182 mg min^{-1}, due to the simultaneous reduction of complex compounds. These data further strengthen the previously described TG analysis, and a collation of both leads to the conclusion that 338.7 °C is the thermal resistance temperature for the Bamboo Apus biomass to be used for resistance during the carbonization process.

3.3 Microstructure analysis

X-ray diffraction is (XRD) a characterization of a materials, in order to determine the microstructure of activated carbon electrodes, including the lattice parameters, layer height (L_c), width (L_a), and number (N_p). Figure 4 shows the XRD curve of activated carbon derived from bamboo apus biomass at 2θ angle with a range of 10°–60°. All samples exhibited two broad peaks in position of 22.33°–25.50° and 43.92°–44.09° which correlated with diffraction planes of 002 and 100. This is confirmed that all samples have carbons with turbostratic (disordered) structures, which indicates that the samples are composed of graphitic-like microcrystallites that are randomly oriented and distributed. This is due to random shifts between adjacent layers, varying interspacing values, unorganized carbon that is not part of the layer structure, and strain in the layers [31]. This phenomenon is related to other previous studies that performed the XRD analysis for activated carbon based on biomass precursor. In addition, increasing the carbonization temperature from 600 to 800 °C could change the 002 reflection plane were moved to the lower angle from 25.50 to 22.33 which indicated a more developed pseudo-crystallite structure. This provided a high active site as well as ion transport pathway at the electrolyte/electrode interface [32]. All these phenomena could enhance supercapacitor performance [33]. Furthermore, the addition of the carbonization temperature up to 900 °C again shifted the wide peak to a slightly larger

Fig. 2 Density shrinkage of the electrodes

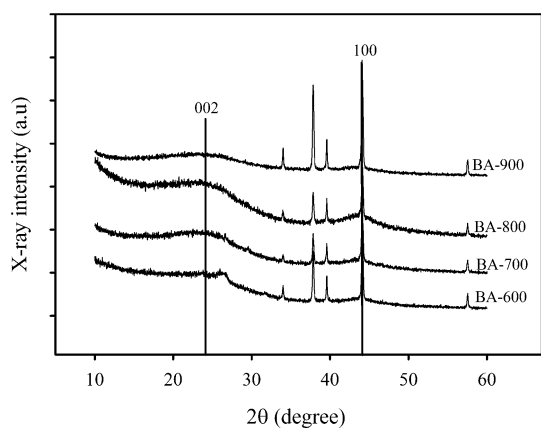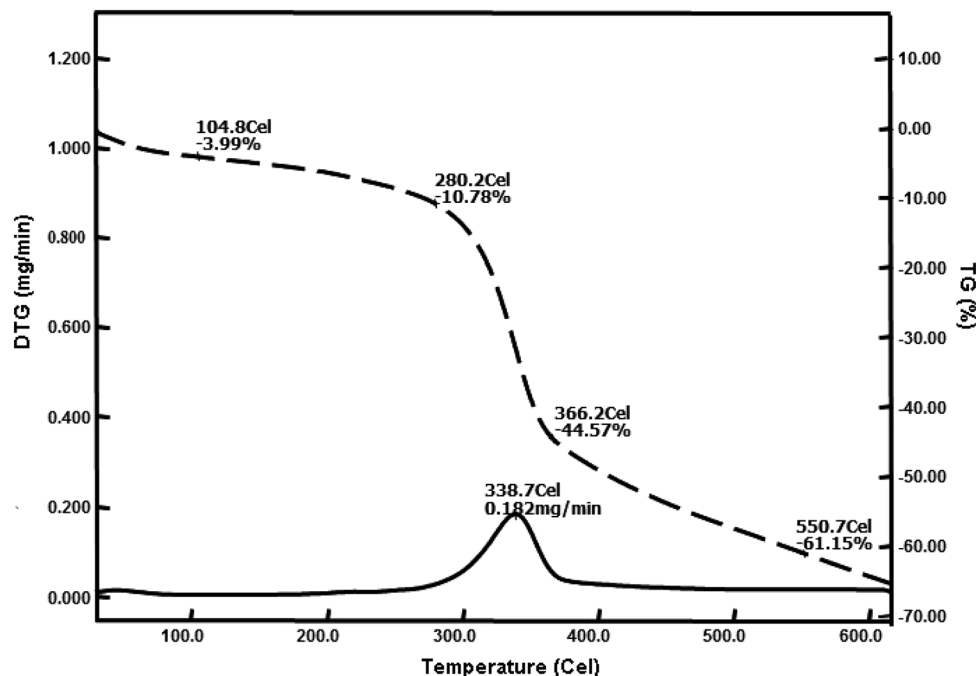**Fig. 3** TG/DTG profiles

Fig. 4 The XRD pattern of all samples

23.11° which indicates a reduction in the pseudo-crystallite structure of carbon. Moreover, the presence of another sharp peak indicates the existence of silica, which is often found in biomass [34].

The characterization of X-ray diffraction produces the lattice parameters of bamboo apus, which is presented in Table 1, along side the microcrystalline dimensions of the supercapacitor cell electrode, including BA-600, Ba-700, BA-800, and BA-900. Based on the data obtained, it was observed that BA-800 and BA-600 samples exhibited the lowest and highest L_c, respectively. In addition, empirical formula is used to analyze the relationship between the dimensions of microcrystallites (L_c) and surface area

[35, 36], which was confirmed to be dependent for all samples. This assumption is evidenced by the largest surface area exhibited by BA-800 and the smallest is seen in BA-600.

3.4 Surface morphology analysis

Figure 5 shows SEM micrographs at a magnification of 5000, and all samples demonstrate evenly spread pores on the surface of the electrode. Conversely, an increase in carbonization temperature leads to the formation of larger-sized pore diameter, and the values recorded for BA-600, Ba-700, BA-800, and BA-900 samples are 0.35 μm, 0.50 μm, 0.44 μm, and 1.05 μm, respectively. In addition, carbon fiber presented in BA-700 and BA-800 samples had an average diameter of 0.17 μm and 0.06 μm, as a clearer surface morphology structure is observed at the higher magnification of 40,000×. Figure 6a shows the domination of BA-600 sample by pores with an average diameter size of 192.21 nm, while carbon fibers with an average diameter of 103.54 nm and 52.07 nm as shown in Fig. 6b and c are prominent in BA-700 and BA-800. In addition, it was also established that sample BA-900 is characterized by larger pore sizes, with an average diameter size of 652.34 nm. Figures 5 and 6 demonstrate the domination of BA-600 and BA-900 samples by carbon pores without the fiber, while BA-700 and BA-800 contains both features.

Table 1 The interlayer spacing parameters and the microcrystalline dimensions of the electrodes

| Sample codes	Interlayer spacing				Microcrystalline dimension		L_c/L_a	N_p
	(002)	(100)	d_{002} (nm)	d_{100} (nm)	L_a (nm)	L_c (nm)		
BA-600	25.50	44.09	3.69	2.04	25.26	27.13	0.85	7.35
BA-700	23.38	44.08	3.85	2.05	10.39	23.87	0.45	6.20
BA-800	22.33	44.08	3.90	2.05	11.23	10.41	0.93	2.67
BA-900	23.11	43.92	4.06	1.98	8.43	25.50	3.02	6.28
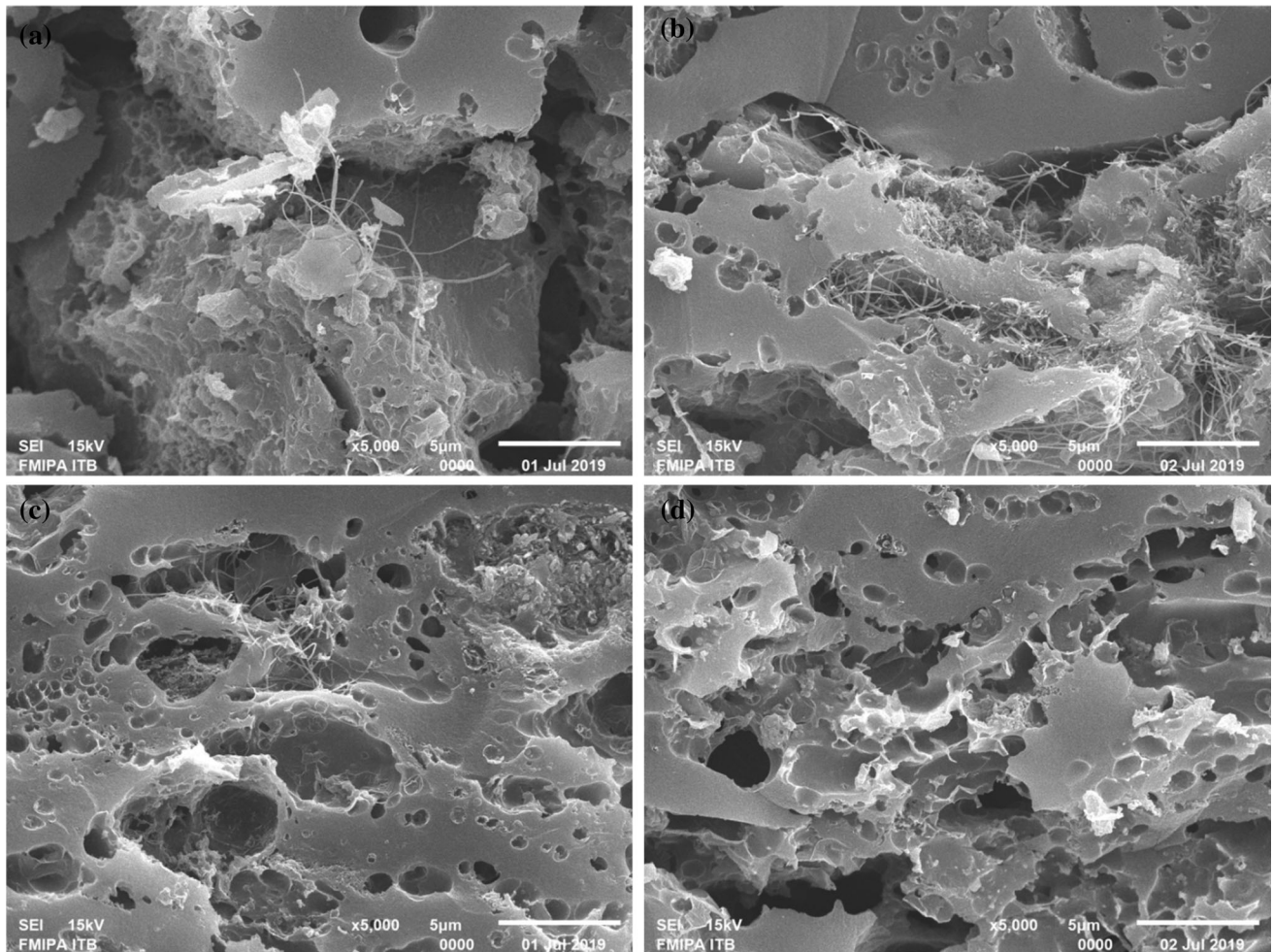
Fig. 5 SEM micrographs at a magnification of ×5000 for **a** AB-600, **b** AB-700, **c** AB-800, and **d** AB-900

Furthermore, an increase in carbonization temperature results in elevation in pore size, due to the fact that carbon tends to break down, leading to the formation of new particles and the enlargement of existing pores [7, 37]. This process also reduces fiber diameter, as the value obtained for sample BA-700 is comparably larger than BA-800. This study confirmed the appearance of carbon fibers only in BA-700 and BA-800 samples, due to the opening of those that were previously closed. However, this characteristic is not present in BA-600, due to fact that it had not formed a fiber, and also BA-900, which is exposed to excess temperatures, subsequently causing the fiber to break down.

3.5 The chemical composition analysis

The EDX characterization of elemental content percentage for carbon (C), oxygen (O_2), silica (Si), and potassium (K) is shown in Fig. 7 and Table 2. In
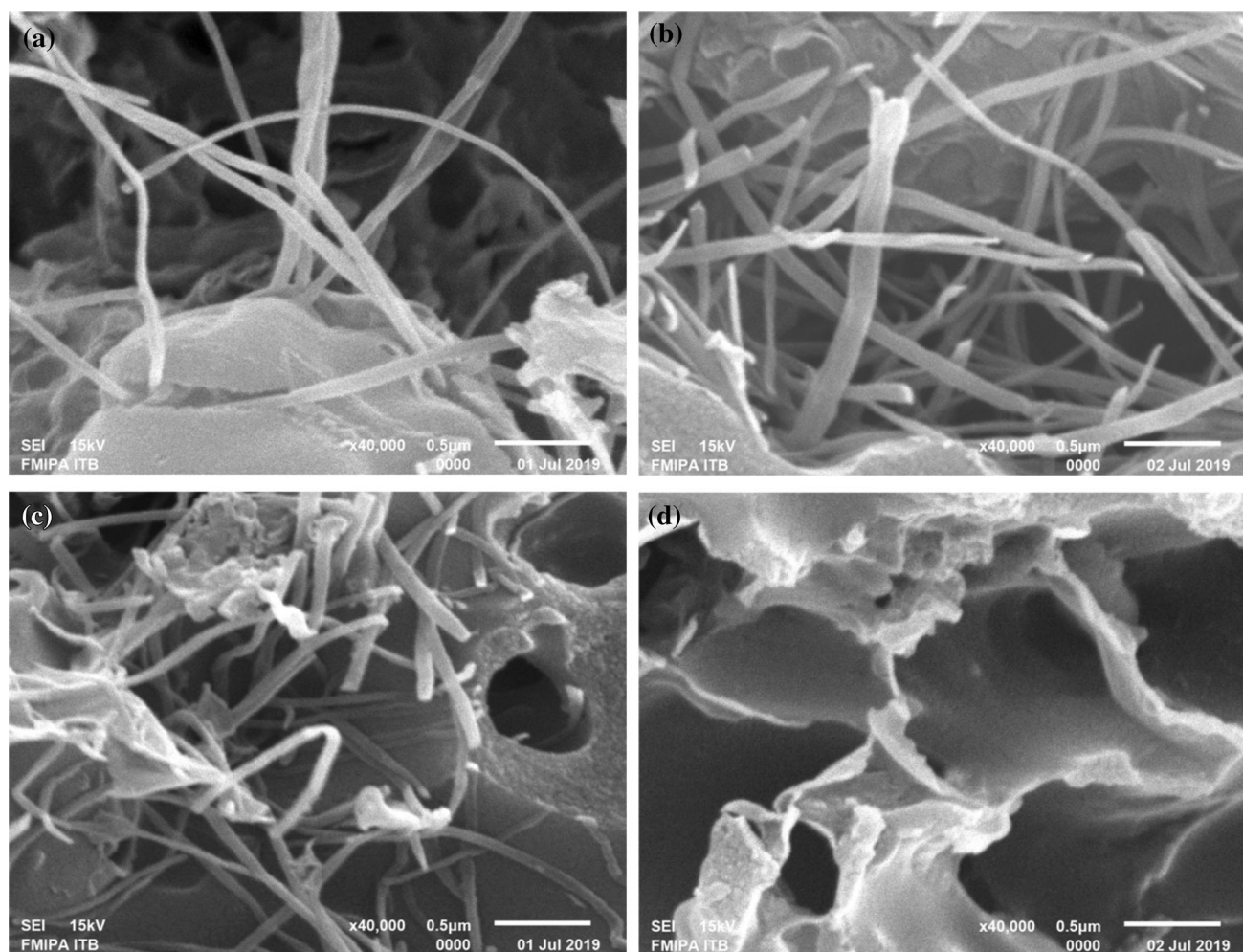
Fig. 6 SEM micrographs at a magnification of ×40,000 for **a** AB-600, **b** AB-700, **c** AB-800, and **d** AB-900

addition, the high carbon peak is an indication of the elevated composition of the electrode. Meanwhile, the appearance of oxygen was due to the formation of bonds between carbon and oxygen in the physical activation process with CO_2 gas, while the presence of silica elements is linked to its occurrence in biomass [38], and potassium element is affiliated with the KOH activators used in chemical activation. The BA-600 sample exhibits magnesium element because of the incomplete evaporation of chlorophyll in bamboo at 600 C. Table 2 shows the largest carbon content in the BA-800 sample, which is directly proportional to the specific capacitance obtained in.

3.6 Porosity properties analysis

The porosity properties of electrodes were analyzed using N_2 gas adsorption/desorption method at 77 K, as shown in Fig. 8, as the relationship between the volume of gas absorption and relative pressure tends to follow IV type isotherm based on the IUPAC classification. This is identical to mesopore structures [39]. The specific surface area of the sample was evaluated using the Brauner Emmet Teller (BET) method, and highest N_2 gas absorption volume (390.4990 cc g^{-1}) observed from the curve was seen in BA-800, compared with other samples, at a relative pressure of 0.9542. This, therefore, indicates a high specific surface area of 1137.86 m^2 g^{-1}, while BA-700 has the least surface area of 961.458 m^2 g^{-1}, as shown by the smallest N_2 gas absorption volume of 337.0450 cc g^{-1} in relative pressure of 0.9537. Figure 9 demonstrates the average radius pore of 2.149 nm, which is within the range of mesopore [40], as well as the presence of small micropore. Therefore, it is important to note the absence of a relationship between the parameter of surface area and the
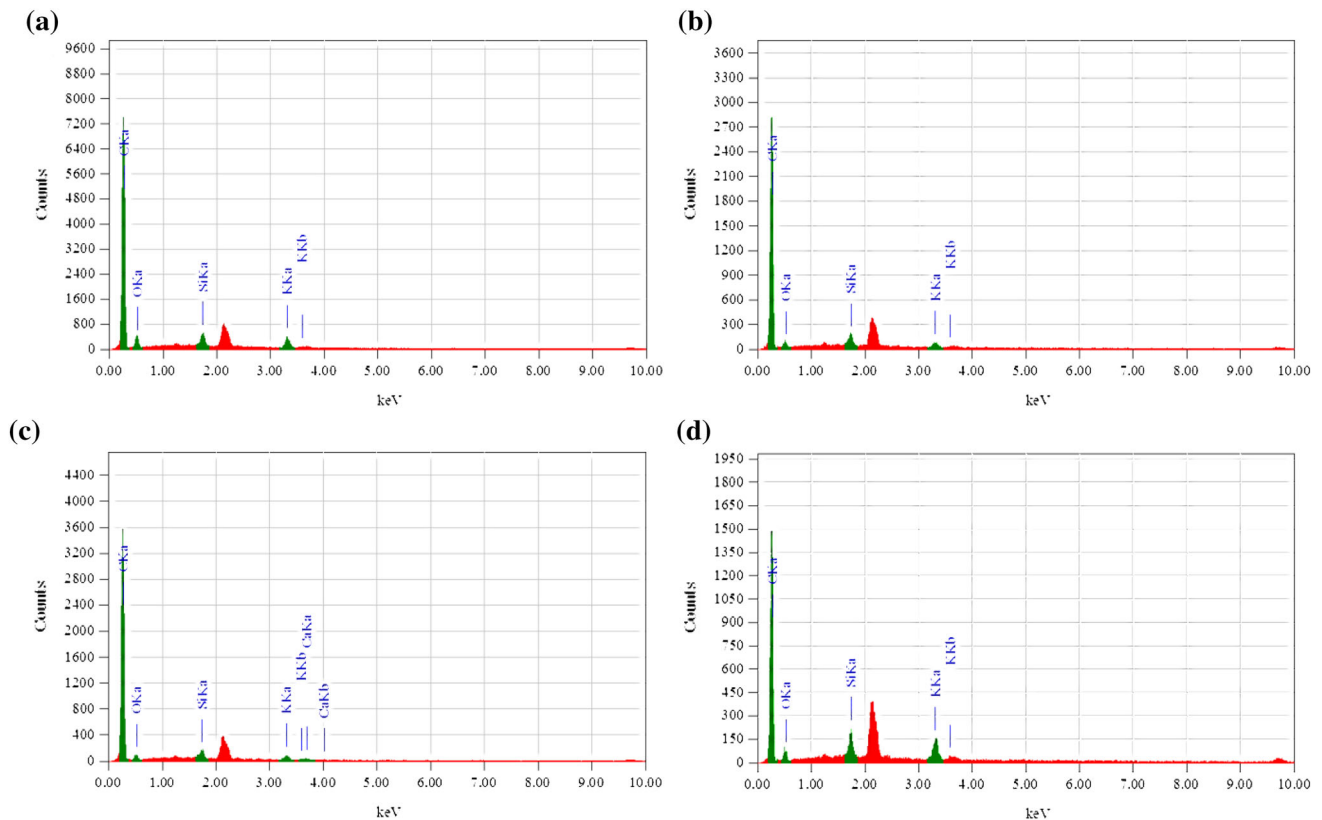
Fig. 7 EDX spectra for **a** AB-600, **b** AB-700, **c** AB-800, and **d** AB-900

Table 2 The elemental composition of carbon electrode made from bamboo waste

| Element contents	Sample codes							
	BA-600		BA-700		BA-800		BA-900	
	Weight (%)	Atoms (%)	Weight (%)	Atoms (%)	Weight (%)	Atoms (%)	Weight (%)	Atoms (%)
Carbon	88.38	92.18	83.04	88.46	89.61	93.18	81.06	88.40
Oxygen	8.44	6.61	12.20	9.76	7.16	5.59	10.04	8.22
Silica	1.07	0.48	1.74	0.79	1.58	0.70	3.05	1.42
Potassium	1.81	0.58	3.02	0.99	1.64	0.52	5.86	1.96
Magnesium	0.30	0.15	–	–	–	–	–	–
Totals	100							

performance of specific capacitances, as some other studies stated the occurrence of inconsistent direct proportionality [41].

3.7 Cyclic voltametry analysis

Cyclic voltametry (CV) is a method used to evaluate capacitive properties, subsequently demonstrating the relationship between current density and voltage window. In addition, the curves obtained for all variations in carbonization temperature present the rectangular shape, which characterized the capacitive electrode properties of the biomass material, as shown in Fig. 10. Also, the width is known to be affected by the charge and discharge current, which indicate the specific capacitance of supercapacitor cells [42]. An increase in carbonization temperature tends to cause an upsurge in the energy-storage
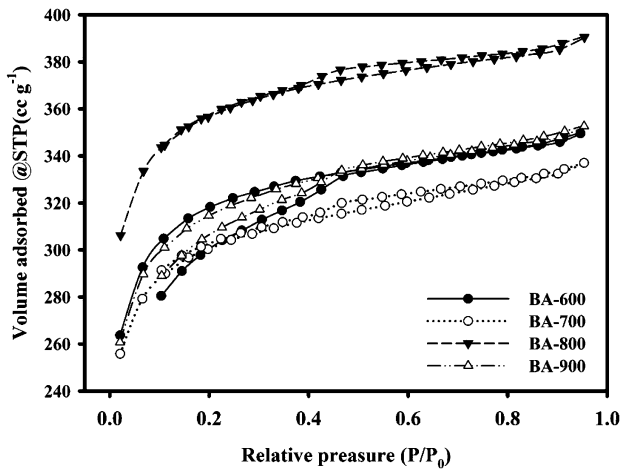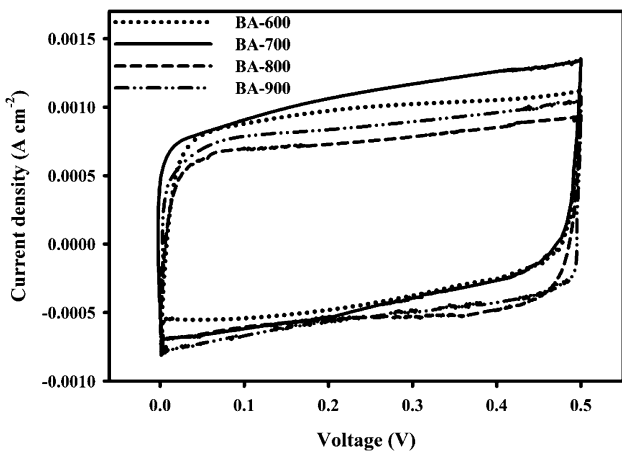
Fig. 8 Nitrogen adsorption desorption isotherms for AB-600, AB-700, AB-800, and AB-900
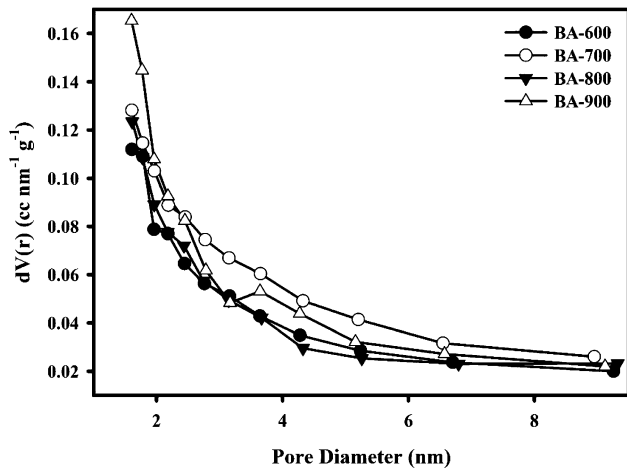
Fig. 9 The pore size distribution for AB-600, AB-700, AB-800, and AB-900

Fig. 10 Cyclic voltammetry curve for all samples

Table 3 The specific capacitance of all electrode supercapacitor based on bamboo waste

Electrode codes	I_c (A)	I_d (A)	Mass (g)	C_{sp} (F g^{-1})
BA-600	0.000604	0.00038	0.0081	121
BA-700	0.001006	0.00045	0.0093	156
BA-800	0.000844	0.00029	0.0065	174
BA-900	0.000634	0.00062	0.0093	135

capacity of supercapacitor electrodes, as evidenced in Fig. 10 and Table 3. Meanwhile, CV curves are observed to increase in size from sample AB-600 to AB-800, indicating an elevation in specific capacitance. The sample BA-800 specifically possessed the largest area, in comparison with others, denoting that the highest electrochemical energy-storage potential occurred in the electrode [43]. In addition, this confirmed the appearance nanofiber structure of BA-800 samples, due to the opening of pores in combination of micro- and mesopores. This is corresponded to the turbostratic (disordered) structures of activated carbon found in the BA-800 sample, as confirmed in a XRD analysis. Furthermore, a reduction in specific capacitance follows the increase in carbonization temperature, as seen in AC-900 electrode, while carbon particles break up larger pores at higher temperatures of 900 °C. This results in enhanced diameter size, causing the production of capacitance by smaller electrodes [44]. Although the highest density reduction occurs at a carbonization temperature of 900, however, the specific capacitance is reduced which indicates that the largest density shrinkage allows the development of pores to a larger direction thereby reducing the surface area and decreasing the capacitive value of the material electrode. In comparison, the specific capacitance produced in this study was almost similar to several previous studies of different precursors such as cotton [5], cow dung [45], and acacia leaves [46] with specific capacitance of 224, 124, and 113 F g^{-1}, respectively.

4 Conclusion

An activated carbon made from bamboo was prepared through the use of different carbonization temperature, and 800 °C was determined to provide

the optimum condition, with high specific capacitance of about 174 F g^{-1}. This excellent electrochemical property is mainly due to the interconnection of porous structure, an increase in surface area to about 1137.86 m^2 g^{-1}, and the high purity of carbon, which promotes ion diffusion to the electrode pores of supercapacitor cell. Therefore, the activated carbon electrode created from bamboo has the potential to be developed as a supercapacitor electrode material.

Acknowledgements

References

1. M. Inagaki, H. Konno, O. Tanaike, J. Power Sources **195**, 7880 (2010)
2. A. Burke, J. Power Sources **91**, 37 (2000)
3. A. González, E. Goikolea, J.A. Barrena, R. Mysyk, Renew. Sustain. Energy Rev. **58**, 1189 (2016)
4. P. González-García, Renew. Sustain. Energy Rev. **82**, 1393 (2018)
5. P. Cheng, T. Li, H. Yu, L. Zhi, Z. Liu, Z. Lei, J. Phys. Chem. C **120**, 2079 (2016)
6. E. Taer, R. Taslim, A.W. Putri, A. Apriwandi, A. Agustino, Int. J. Electrochem. Sci. **13**, 12072 (2018)
7. A. Volperts, G. Dobele, A. Zhurinsh, D. Vervikishko, E. Shkolnikov, J. Ozolinsh, New Carbon Mater. **32**, 319 (2017)
8. C.S. Yang, Y.S. Jang, H.K. Jeong, Curr. Appl. Phys. **14**, 1616 (2014)
9. G. Zhang, Y. Chen, Y. Chen, H. Guo, Mater. Res. Bull. **102**, 391 (2018)
10. B. Sharma, D.U. Shah, J. Beaugrand, E.R. Janeček, O.A. Scherman, M.H. Ramage, Cellulose **25**, 3255 (2018)
11. M.A. Azeez, J.I. Orege, in Bamboo—Current and Future Prospects ed. by H.P.S. Abdul Khalil (Intechopen, Ado Ekiti, 2018), pp. 25–48
12. E. Taer, L. Pratiwi, A. Apriwandi, W.S. Mustika, R. Taslim, A. Agustino (2020) Commun. Sci. Technol. **5**, 22
13. E. Azwar, W.A. Wan Mahari, J.H. Chuah, D.V.N. Vo, N.L. Ma, W.H. Lam, S.S. Lam, Int. J. Hydrog. Energy **43**, 20811 (2018)
14. W. Yang, Z. Shi, H. Guo, J. Guo, X. Lei, L. Yue, Int. J. Electrochem. Sci. **12**, 5587 (2017)
15. H. Hou, D.H. Reneker, Adv. Mater. **16**, 69 (2004)
16. E.J. Ra, E. Raymundo-Piñero, Y.H. Lee, F. Béguin, Carbon N. Y. **47**, 2984 (2009)
17. K. Xu, S. Li, J. Yang, J. Hu, J. Colloid Interface Sci. **513**, 448 (2018)
18. L.F. Chen, X.D. Zhang, H.W. Liang, M. Kong, Q.F. Guan, P. Chen, Z.Y. Wu, S.H. Yu, ACS Nano **6**, 7092 (2012)
19. E.E. Miller, Y. Hua, F.H. Tezel, J. Energy Storage **20**, 30 (2018)
20. Y. Liu, J. Chen, B. Cui, P. Yin, C. Zhang, J. Carbon Res. **4**, 53 (2018)
21. H. Yang, S. Ye, J. Zhou, T. Liang, Front. Chem. **7**, 1 (2019)
22. K. Wang, N. Zhao, S. Lei, R. Yan, X. Tian, J. Wang, Y. Song, D. Xu, Q. Guo, L. Liu, Electrochim. Acta **166**, 1 (2015)
23. E. Taer, A. Apriwandi, Y.S. Ningsih, R. Taslim, A. Agustino, Int. J. Electrochem. Sci. **14**, 2462 (2019)
24. E. Taer, A. Afrianda, A. Apriwandi, R. Taslim, A. Agustino, A. Awitdrus, R. Farma, Int. J. Electrochem. Sci. **13**, 10688 (2018)
25. E. Taer, A. Apriwandi, R. Taslim, U. Malik, Z. Usman, Int. J. Electrochem. Sci. **14**, 1318 (2019)
26. Z. Gao, Y. Zhang, N. Song, X. Li, Mater. Res. Lett. **5**, 69 (2017)
27. J. Jose, V. Thomas, V. Vinod, R. Abraham, S. Abraham, J. Sci. Adv. Mater. Devices **4**, 333 (2019)
28. Y. Fan, Y. Cai, X. Li, L. Jiao, J. Xia, X. Deng, Energy Convers. Manag. **138**, 106 (2017)
29. J. Gonzalez, S. Roma, J.M. Encinar, G. Martı, J. Anal. Appl. Pyrolysis **85**, 134 (2009)
30. M.Y. De Luna, P.M. Rodrigues, G. Antônia, M. Torres, J. Antônio, M.J. Queiroz, M.S. Elaine, R. Maria, A. De Sousa, Energy Sources Part A Recover. Util. Environ. Eff. **41**, 1557 (2018)
31. B.S. Girgis, Y.M. Temerk, M.M. Gadelrab, I.D. Abdullah, Carbon Sci. **8**, 95 (2007)
32. E. Taer, A. Apriwandi, R. Taslim, A. Agutino, D.A. Yusra, J. Mater. Res. Technol. **9**, 13332 (2020)
33. S. Kumagai, M. Sato, D. Tashima, Electrochim. Acta **114**, 617 (2013)
34. L. Wan, P. Song, J. Liu, D. Chen, R. Xiao, Y. Zhang, J. Chen, M. Xie, C. Du, J. Power Sources **438**, 227013 (2019)
35. K. Kumar, R.K. Saxena, R. Kothari, D.K. Suri, N.K. Kaushik, J.N. Bohra, Carbon N. Y. **35**, 1842 (1997)
36. M. Deraman, R. Daik, S. Soltaninejad, N.S.M. Nor, A. Awitdrus, R. Farma, N.F. Mamat, N.H. Basri, M.A.R. Othman, Adv. Mater. Res. **1108**, 1 (2015)
37. J.O. Otulana, O.O. Oluwole, Int. J. Nov. Res. Eng. Sci. **2**, 1 (2016)
38. S. Sugashini, K.M.M.S. Begum, Xinxing Tan Cailiao/New Carbon Mater. **30**, 252 (2015)
39. K.S.W. Sing, Pure Appl. Chem. **54**, 2201 (1982)

40. S. Ahmed, A. Ahmed, M. Rafat, J. Saudi Chem. Soc. **22**, 993 (2018)

41. L. Muniandy, F. Adam, A. Rahman, E. Ng, Microporous Mesoporous Mater. **197**, 316 (2014)

42. K. Scott, *Electrochemical Principles and Characterization of Bioelectrochemical Systems* (Elsevier Ltd., Newcastle upon Tyne, 2016).

43. A. Bakandritsos, P. Jakubec, M. Pykal, M. Otyepka, FlatChem **13**, 25 (2019)

44. P. Poonam, K. Sharma, A. Arora, S.K. Tripathi, J. Energy Storage **21**, 801 (2019)

45. D. Bhattacharjya, J.S. Yu, J. Power Sources **262**, 224 (2014)

46. E. Taer, K. Natalia, A. Apriwandi, R. Taslim, A. Agustino, R. Farma, Adv. Nat. Sci. Nanosci. Nanotechnol. **11**, 25007 (2020)